SCIENTIA PLENA
www.scientiaplena.org.br
VOL. 21, NUM. 03 2025
doi: 10.14808/sci.plena.2025.034201

Application of Advanced Numerical Methods to Solve the Batch Sedimentation Problem: Tangent of Hyperbola Interface Capturing, Weighted Essentially Non-Oscillatory and High-Resolution Central Scheme

Aplicação de Métodos Numéricos Avançados para Resolver o Problema de Sedimentação Batelada: Captura de Interface por Tangente Hiperbólica, Essencialmente Não-Oscilatório Ponderado e Esquema Central de Alta Resolução

F. S. Lobato; F. M. Fagundes*; J. J. R. Damasceno; F. O. Arouca

Faculdade de Engenharia Química, Universidade Federal de Uberlândia, Av. João Naves de Ávila, 2121, Bairro Santa Mônica, 38400-902, Uberlândia/MG, Brasil.

* flaviamfagundes@gmail.com
(Recebido em 17 de janeiro de 2025; aceito em 31 de março de 2025)

The numerical solution of the sedimentation phenomenon presents a significant challenge due to the presence of discontinuities at interfaces, characterized by three distinct regions: (i) clear liquid, (ii) constant solid concentration, and (iii) solid concentration varying from the initial to a maximum value. This problem is particularly relevant in the oil industry, where sedimentation is an essential unit operation in processes such as wastewater treatment, drilling fluid control, and phase separation during production. Discontinuities and abrupt variations in solid concentrations pose significant challenges for traditional numerical methods in solving this model type. In this study, three high-order numerical methods (Tangent of Hyperbola Interface Capturing, Weighted Essentially Non-Oscillatory, and High-Resolution Central Scheme) are employed to solve two classic case studies in the sedimentation process. In general, the results indicate that all three methods were effective in handling the discontinuities at the phase interfaces while maintaining the accuracy and stability of the solution. Moreover, although all methods performed satisfactorily in various aspects, the High-Resolution Central Scheme was found to be the most efficient in terms of computational time.
Keywords: sedimentation, discontinuity, high-resolution schemes.

A resolução numérica do fenômeno de sedimentação configura um grande desafio devido à presença de descontinuidades nas interfaces caracterizadas por três regiões distintas, a saber, (i) livre de sólidos; (ii) concentração de sólidos constante e (iii) concentração de sólidos varia de um valor inicial até um valor máximo. Este problema é particularmente relevante na indústria de petróleo, onde essa operação unitária é essencial em processos como o tratamento de águas residuais, controle de fluidos de perfuração e separação de fases durante a produção. A presença de descontinuidades e variações abruptas nas concentrações de sólidos apresenta desafios significantes para os tradicionais métodos numéricos usados para resolver este tipo de modelo. Nesta contribuição, três métodos numéricos com alta ordem, a saber, Captura de Interface por Tangente Hiperbólica, Essencialmente Não-Oscilatório Ponderado e Esquema Central de Alta Resolução são empregados para a resolução de dois estudos de caso clássicos no processo de sedimentação. Em geral, os resultados indicam que todos os três métodos foram eficazes no tratamento das descontinuidades nas interfaces de fase, mantendo a precisão e a estabilidade da solução. Além disso, embora todos os métodos tenham tido um desempenho satisfatório em vários aspectos, o Esquema Central de Alta Resolução foi considerado o mais eficiente em termos de tempo computacional.
Palavras-chave: sedimentação, descontinuidade, esquemas de alta resolução.

1. INTRODUCTION

Sedimentation is a natural or induced physical process involving the transport and deposition of suspended particles in a fluid [1]. The phenomenon of sedimentation is widely used in various industries, including the oil industry, where its applicability can be highlighted in wastewater treatment, drilling fluid quality control, and phase separation processes in production and refining [2]. Sedimentation depends on factors such as particle size, shape, and density, as well as fluid

properties. Larger and denser particles settle more quickly, while smaller or less dense particles remain suspended for a longer time. The particles suspended in a fluid move due to forces such as gravity, drag force generated by the fluid's viscosity, and buoyant force [1].

One of the main advantages of this process is its efficiency and relatively low cost compared to filtration and centrifugation. Additionally, it is important to note that sedimentation does not require the use of additional chemicals, thus reducing operational costs. Regarding energy requirements, this unit operation is passive, relying on gravity, unlike other separation processes. This makes it a more energy-efficient alternative, especially for treating large volumes of fluid. On the other hand, its limitations include low efficiency for treating very small or low-density particles, which can result in extended operational times. The sedimentation tank may also require a very large space to treat significant volumes. Finally, although the process is simple, it may require continuous monitoring to ensure proper particle separation. This may involve maintaining optimal conditions in the fluid, such as viscosity and temperature, as well as controlling suspension characteristics, such as solid concentration [1-3].

From a mathematical perspective, the numerical modeling of the sedimentation process presents significant challenges. This is due to the complexity of the phenomenon, which involves interactions between particles, external forces, turbulence, and compaction effects, as well as the presence of discontinuities and abrupt variations in solid concentrations [4-7]. In this context, traditional approaches such as Finite Difference, Finite Volume, and Finite Element methods may encounter difficulties related to accuracy and the treatment of discontinuities if they are not paired with appropriate techniques to discretize the advective and diffusive terms present in phenomenological models [8].

To overcome or minimize the impact of these difficulties, numerical methods known as high-resolution schemes for dealing with nonlinear convective-diffusive terms have been proposed. The first scheme with this goal was proposed by Lax–Friedrichs (1954) [9]. Since then, several other schemes for this purpose have been developed. Total Variation Diminishing (TVD) schemes, such as the MUSCL (Monotone Upstream-centered Schemes for Conservation Law) scheme, can handle discontinuities without numerical oscillations by introducing slope or flux limiters, although they typically suffer from excessive numerical dissipation [10]. Nessyahu and Tadmor (1990) [11] proposed a central scheme that offers higher resolution than that developed by Lax–Friedrichs, while maintaining the simplicity of the approach without a Riemann solver. Liu et al. (1994) [12] proposed a new shock-capturing scheme called the Weighted Essentially Non-Oscillatory (WENO) strategy. The goal is to use a convex combination of all points to achieve the essentially non-oscillatory property, while also improving accuracy by one order. As a result, these schemes are based on cell averages and a total variation diminishing Runge-Kutta time discretization. Bürger and Concha (1998) [4] proposed a numerical scheme based on a non-oscillatory central difference method combined with a minmod limiter to control the flux. Kurganov and Tadmor (2000) [8] introduced a new family of central schemes called High-Resolution Central Scheme (HRCS) that retain the simplicity of being independent of the problem's self-structure while enjoying much lower numerical viscosity compared to the approaches proposed by Lax–Friedrichs (1954) [9] and Nessyahu and Tadmor (1990) [11]. The main idea behind these central schemes is the use of more accurate information about local propagation velocities. It is worth noting that this scheme admits a particularly simple semi-discrete formulation.

Xiao et al. (2005) [13] proposed a simple and practical scheme called Tangent of Hyperbola Interface Capturing (THINC) for capturing moving interfaces or free boundaries in multi-phase simulations. This scheme uses the hyperbolic tangent function to calculate the numerical flux of the volume fraction function, providing a conservative, oscillation-free, and smearing-free solution for the volume fraction function, even for extremely distorted interfaces of arbitrary complexity. Bürger et al. (2008) [14] introduced a new family of numerical schemes to handle differential problems with discontinuous fluxes using a MUSCL approach combined with a Runge-Kutta time discretization to achieve second-order accuracy. Bürger et al. (2009) [15], Wang et al. (2010) [16] and Bürger et al. (2020) [17] proposed the Engquist-Osher scheme with extrapolation and flux-limiting functions to solve nonlinear convective equations. Diehl (2007) [18] estimated the batch-settling flux function for an ideal suspension from only two experiments considering the Godunov's method. Bürger et al. (2013) [19] proposed a robust numerical method

to control discontinuities based on use of constitutive relations for hindered settling, compression and dispersion and the Godunov's method. This same numerical approach was used to Diehl (2015) [20] to identify constitutive functions in scalar nonlinear convection–diffusion equations applied to batch sedimentation. In similar way, Rocha et al. (2020) [21] determine constitutive equations in the sedimentation process for thickened and clarified regions separately.

In this work, three high-resolution numerical techniques (THINC, WENO and HRCS) are evaluated to solve the sedimentation problem. The aim is to assess whether these approaches are capable of handling discontinuities at the interfaces and ensuring the accuracy and stability of the solution during the integration of the partial differential model. For this purpose, two classical sedimentation problems are considered.

This paper is organized as follows. Section 2 revisits the concepts of the sedimentation process, with a focus on its mathematical modeling. Section 3 provides a brief description of the THINC, WENO and HRCS strategies. Section 4 presents the numerical results considering a purely mathematical case study with an analytical solution to validate the methodologies, followed by two sedimentation case studies. Finally, the conclusions are presented in the last section.

2. MATHEMATICAL MODELING

As mentioned earlier, the sedimentation process is a complex phenomenon that describes the settling dynamics of particulate materials. From a physical point of view, sedimentation is a process by which solid particles suspended in a liquid or gas settle at the bottom of a container. This process occurs due to the action of gravity, which causes the heavier particles to settle first. The duration of this process can range from hours to days or even weeks, depending on the size and density of the particles involved. There are different types of sedimentation, depending on the characteristics of the particles and the environmental conditions. Some of the main types of sedimentation include gravitational sedimentation, centrifugation, and filtration sedimentation. Each of these processes has its own specific characteristics and applications [1-3, 22].

Fagundes et al. (2021) [23] describes the phenomenon of batch sedimentation along the time t as a moving boundary problem, where discontinuities move through space, delineating three distinct regions: (i) clear region (Region I: the local volumetric concentration of the solid phase (ε_s) is equal to zero); (ii) free settling region (Region II: ε_s is equal to initial volumetric concentration (ε_{s0})); and (iii) compression region (Region III: $\varepsilon_{s0} < \varepsilon_s \leq \varepsilon_{sm}$, where ε_{sm} is the maximum volumetric concentration).

Figure 1 presents the problem of subdomains with moving boundaries, represented by the descending and ascending interfaces on the z-axis, labeled by indices (1,2) and (3,4), respectively, with the origin of the positions at its base and the maximum height of the suspension at $z=L$ (L is the length of the sedimentation column).

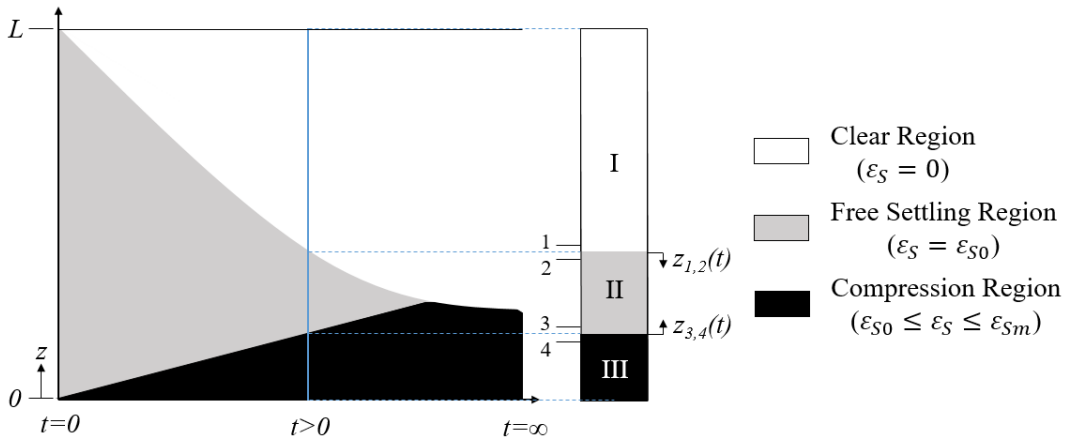

Figure 1: Regions I, II and III of batch sedimentation delimited by discontinuities: descending interface (1,2) and ascending interface (3,4).

It is important to mention that the predicted discontinuities are singular surfaces that move through the spatial domain as functions of time, with $z_{1,2}(t)$ and $z_{3,4}(t)$ representing the positions of the descending and ascending interfaces, respectively, at a given time t. As mentioned by Fagundes et al. [23], each region delimited by discontinuities can be modeled separately using the continuity and motion equations derived from mixture theory, in addition to incorporating the appropriate constitutive equations for each case. For this purpose, Bürger and Wendland (1998) [24] developed the entropy boundary and jump conditions for the sedimentation problem considering compression. These conditions can be used to delimit each region during the simulation of the process.

Mathematically, the sedimentation process is modeled considering the continuity and linear momentum equations. For a transient and unidirectional flow with density of solids constant, the set of equations for the solid phase is given by [4]:

$$\frac{\partial \varepsilon_s}{\partial t} + \frac{\partial \left(v_s \varepsilon_s \right)}{\partial z} = 0 \tag{1}$$

$$\rho_s \varepsilon_s \left(\frac{\partial v_s}{\partial t} + v_s \frac{\partial v_s}{\partial z} \right) = \frac{\partial T_s}{\partial z} + m_z + \varepsilon_s \left(\rho_s - \rho_f \right) g_z \tag{2}$$

$$\varepsilon_s = \varepsilon_{s0}, \quad t=0 \text{ and } 0 \le z \le L \tag{3}$$

$$v_s \varepsilon_s = 0, \quad t > 0 \text{ and } z=0 \tag{4}$$

$$v_s \varepsilon_s = 0, \quad t > 0 \text{ and } z=L \tag{5}$$

where v_s is the velocity of the solid phase, ρ_s and ρ_f represent the densities of the solid and liquid phases, respectively, T_s is the stress tensor of the solid phase, m_z is the resistive force and g_z is the gravitational acceleration.

To solve this model, it is necessary to define constitutive equations, used to characterize the material properties of the solid and liquid constituents of the suspension, as well as the stress tensor of the solid phase and the resistive force. An important simplification can be applied in this model [4-6, 20]. These works demonstrated that the inertial terms (local acceleration and convective flux of linear momentum) can be neglected in Eq. (2) when compared with other terms acting on the physical system. Based on this hypothesis, the velocity of the solid phase can be represented by an algebraic equation as a function of the local volumetric concentration of the solid phase and constitutive equations. Thus, Eq. (2) can be rewritten as:

$$v_s = g(\varepsilon_s) \tag{6}$$

were $g(\varepsilon_s)$ is an expression that relates how velocity is a function of the solids concentration.

As a consequence of this hypothesis, the original model can be represented by the following partial differential equation:

$$\frac{\partial \varepsilon_s}{\partial t} + \frac{\partial \left(g(\varepsilon_s) \varepsilon_s \right)}{\partial z} = 0 \tag{7}$$

subject to initial and boundary conditions.

It is important to mention that, although the model has been simplified, the difficulties related to discontinuities and abrupt variations in the solids concentration profile and discontinuities in the solids density flux ($g(\varepsilon_s)\varepsilon_s$) are still present [4-6, 17, 20]. In this case, to solve a model with these characteristics, numerical methods capable of overcoming or minimizing such obstacles must be employed.

3. NUMERICAL METHODS

As mentioned earlier, the sedimentation process can be represented by Eq. (7). In order to present the numerical methods considered to solve this partial differential equation (PDE), consider the following Cauchy problem for scalar conservation laws:

$$\frac{\partial u}{\partial t}+\frac{\partial f(u)}{\partial z}=0 \tag{8}$$

where t is the time, z is the spatial variable, u is the dependent variable and $f(u)$ is a mathematical expression defined in terms of the dependent variable.

This type of hyperbolic problem commonly appears in case studies involving fluid dynamics, wave propagation, and the modeling of phenomena with discontinuities [4, 5]. In this case, traditional numerical methods such as Finite Difference, Finite Volume and Finite Element Methods may be ineffective or inaccurate when applied to these problems due to numerical oscillations or loss of precision in the discontinuity regions [8]. Thus, it is necessary to employ numerical strategies that can accurately capture the abrupt transitions in the solution, such as shock waves, interface fronts, and other discontinuities [4, 5, 8].

In the next sections, a brief description of Tangent of Hyperbola Interface Capturing (THINC), Weighted Essentially Non-Oscillatory (WENO) and High-Resolution Central Scheme (HRCS) strategies considered to solve Eq. (8) are presented.

3.1 Tangent of Hyperbola Interface Capturing

The Tangent of Hyperbola Interface Capturing (THINC), proposed by Xiao et al. (2005) [13], configures an efficient and accurate approach for solving PDEs with discontinuities, while maintaining conservation and numerical stability. The main idea is to approximate the solution $u(t,z)$ by considering a smooth hyperbolic profile to represent the transition between different solution regions. Thus, the solution at the (n+1)-th time step is given by:

$$u_i^{n+1}=u_i^n-\frac{\Delta t}{\Delta z}\left(f_{i+1/2}-f_{i-1/2}\right) \tag{9}$$

where $f_{i+1/2}$ is the flux transported across boundary $x_{i+1/2}$ during the interval Δt, and computed as:

$$f_{i+1/2}=\begin{cases}-\int_{t^n}^{t^{n+1}}\Theta_i\left(z_{i+1/2}-u_{i+1/2}\left(\tau-t^n\right)\right)u d\tau, & \text{if } u_{i+1/2}\geq 0\\ \int_{t^n}^{t^{n+1}}\Theta_{i+1}\left(z_{i+1/2}-u_{i+1/2}\left(\tau-t^n\right)\right)u d\tau, & \text{otherwise}\end{cases} \tag{10}$$

where $\Theta_i(Z)$ is the reconstruction interpolation function.

The THINC scheme uses the piecewise hyperbolic tangent function:

$$\Theta_i(Z)=\frac{1}{2}\left(1+\gamma\tanh\left(\beta\left(\frac{Z-x_{i-1/2}}{\Delta z}-\tilde{Z}_i\right)\right)\right) \tag{11}$$

where γ is equal to 1 for $u_{i-1}<u_{i+1}$ and γ is equal to -1 for $u_{i-1}>u_{i+1}$. β (=1.5) is a parameter defined to control the slope and the thickness of the jump. The value of the $\tilde{Z}_i$ parameter is computed as:

$$\tilde{Z}_i=\frac{1}{2\beta}\ln\left(\frac{\exp\left(\frac{\beta}{\gamma}\left(1+\gamma-2u_i\right)\right)-1}{1-\exp\left(\frac{\beta}{\gamma}\left(1+\gamma-2u_i\right)\right)}\right) \tag{12}$$

According to Xiao et al. (2005) [13], the main advantages of the THINC strategy are: (a) high precision in capturing interfaces: the use of the hyperbolic tangent provides a smooth and accurate transition between regions with different solution behaviors, which is particularly useful for capturing shock waves or phase transitions with high resolution; (b) numerical stability: the approach preserves stability even when the solution involves strong discontinuities; and (c) flexibility: this numerical strategy is applicable to a wide range of problems in fluid dynamics, compressible flows, and multi-phase simulations, making it a robust tool for handling problems with complex interfaces. In the specialized literature, different applications involving the THINC

strategy can be found, such as solution of multi-dimensional test cases [25, 26]; simulations of multi-phase interfacial flows in the presence of complex geometrical configuration [27]; and compressible gas dynamics with reactive fronts [28].

3.2 Weighted Essentially Non-Oscillatory

The Weighted Essentially Non-Oscillatory (WENO) is a numerical approach proposed by Liu et al. (1994) [12] and utilized to solve PDE that involve discontinuities or abrupt transitions in the solutions. As mentioned by Jiang and Shu (1996) [29], this method is particularly effective in problems with compressible flows, shock waves, and other physical phenomena that exhibit discontinuities or irregular characteristics. In addition**,** WENO stands out for its ability to ensure precise and robust resolution, maintaining numerical stability and avoiding unwanted oscillations in the discontinuity regions [30].

In general, WENO is based on the concept of a weighted average of local approximations, where contributions from different stencils (interpolation patterns) are weighted to minimize oscillations in regions with discontinuities while maintaining a high order of accuracy in smooth regions [12]. From a mathematical perspective, the flux *f(u)* at each mesh point is calculated using the weighted combination formula given by:

$$f(u) \approx \frac{1}{\Delta z}\left(f_{R(i+1/2)} - f_{L(i-1/2)} \right) \tag{13}$$

where $f_{L(i\text{-}1/2)}$ and $f_{R(i+1/2)}$ are the local approximation of the flux, computed, as example, the fifth order finite difference WENO scheme has the flux given by:

$$f_{R(i+1/2)}(u) = \omega_1 f^{(1)}_{R(i+1/2)} + \omega_2 f^{(2)}_{R(i+1/2)} + \omega_3 f^{(3)}_{R(i+1/2)} \tag{14}$$

where the three third order fluxes on three different stencils are given by:

$$f^{(1)}_{R(i+1/2)} = \frac{1}{3} f(u_{i-2}) - \frac{7}{6} f(u_{i-1}) + \frac{11}{6} f(u_i) \tag{15}$$

$$f^{(2)}_{R(i+1/2)} = -\frac{1}{6} f(u_{i-1}) + \frac{5}{6} f(u_i) + \frac{1}{3} f(u_{i+1}) \tag{16}$$

$$f^{(3)}_{R(i+1/2)} = \frac{1}{3} f(u_i) + \frac{5}{6} f(u_{i+1}) - \frac{1}{6} f(u_{i+2}) \tag{17}$$

The weights w_i are given by:

$$w_i = \frac{\tilde{w}_i}{\sum_{k=1}^{3} \tilde{w}_k} \tag{18}$$

$$\tilde{w}_k = \frac{\gamma_k}{\left(\beta_k + \sigma\right)^2} \tag{19}$$

where γ_1=1/10, γ_2=3/5 and γ_3=3/10.

The smoothness indicators β_k given by:

$$\beta_1 = \frac{13}{12}\left(f(u_{i-2}) - 2f(u_{i-1}) + f(u_i) \right)^2 + \frac{1}{4}\left(f(u_{i-2}) - 4f(u_{i-1}) + 3f(u_i) \right)^2 \tag{20}$$

$$\beta_2 = \frac{13}{12}\left(f(u_{i-1}) - 2f(u_i) + f(u_{i+1}) \right)^2 + \frac{1}{4}\left(f(u_{i-1}) - 4f(u_{i+1}) \right)^2 \tag{21}$$

$$\beta_3 = \frac{13}{12}\left(f(u_i) - 2f(u_{i+1}) + f(u_{i+2}) \right)^2 + \frac{1}{4}\left(3f(u_i) - 4f(u_{i+1}) + f(u_{i+2}) \right)^2 \tag{22}$$

Finally, σ is a small parameter that prevents division by zero ($\approx 10^{-10}$). The WENO method uses an iterative procedure to dynamically adjust the weights w_i, ensuring that the solution optimally adapts to the presence of discontinuities [12].

For a first-order finite difference scheme, the approximation u is given by:

$$u_i^{n+1} = u_i^n - \frac{\Delta t}{\Delta z} f\left(u_i^n\right) \tag{23}$$

The WENO method offers several advantages, particularly for problems involving discontinuities or compressible flows [12]: (a) high precision in smooth regions and near discontinuities: this approach ensures high-order resolution in smooth regions of the solution and captures discontinuities without oscillations, maintaining high-order accuracy in non-discontinuous regions; (b) numerical stability: the method is designed to avoid unwanted oscillations in discontinuity regions, a common issue in traditional finite difference schemes; and (c) flexibility: WENO can be adapted to a wide range of PDE problems, being particularly useful for compressible flows, fluid dynamics, shock wave problems, and multi-phase interfaces.

The WENO scheme has been used to solve problems in different areas, such as case studies involving PDEs and non-PDE problems [31, 32]; nonlinear hyperbolic conservation laws [33]; and modeling cavitation induced by an underwater explosion [34].

3.3 High-Resolution Central Scheme

The High-Resolution Central Scheme (HRCS), proposed by Kurganov and Tadmor [8], represents a class of numerical strategies used to solve hyperbolic partial differential equations, particularly in problems involving discontinuities. These schemes are designed to solve conservative partial differential equations robustly and accurately, using a combination of central finite difference techniques and high-order resolution approaches, without the need for explicit solution reconstruction or large-scale smoothing operations.

These schemes are characterized by their use of central fluxes and the implementation of a high-order resolution approach, meaning that, unlike conventional methods, HRCS do not rely on gradient interpolation of the solution but instead on an implicit reconstruction of the flux. This allows for more accurate capturing of discontinuities with high-order precision.

In general terms, the central idea behind HRCS is the use of a central finite difference formula for the discretization of the divergence term ($\partial f(u)/\partial z$), combined with a flux averaging technique to update the solution values at the control volumes. The flux is computed to ensure the equation is solved conservatively and accurately, even in the presence of discontinuities [8].

For a control volume i (discretization in space), the solution update at time n+1 is given by:

$$w_i^{n+1} = u_i^n + \Delta t\left(\frac{H_{i+1/2}\left(u^n\right) - H_{i-1/2}\left(u^n\right)}{\Delta z}\right) \tag{24}$$

$$u_i^{n+1} = \frac{u_i^n}{2} - \frac{1}{2}\left(w_i^n + \Delta t\left(\frac{H_{i+1/2}\left(w^n\right) - H_{i-1/2}\left(w^n\right)}{\Delta z}\right)\right) \tag{25}$$

where $H_{i+1/2}$ and $H_{i\text{-}1/2}$ represents the centrally located fluxes at the interfaces between cells i e i+1, and Δz and Δt are the step size in space and time, respectively. H is computed as:

$$H_{i\pm1/2} = \frac{1}{2}\left(f\left(u_{i\pm1/2}^-\right) + f\left(u_{i\pm1/2}^+\right)\right) - \frac{\lambda_{i\pm1/2}^n}{2}\left(u_{i\pm1/2}^+ - u_{i\pm1/2}^-\right) \tag{26}$$

where the local maximal speeds (λ) can be easily evaluated by following expression:

$$\lambda_{i\pm1/2}^n = \max\left\{\frac{\partial f}{\partial u}\left(u_{i\pm1/2}^-\right), \frac{\partial f}{\partial u}\left(u_{i\pm1/2}^+\right)\right\} \tag{27}$$

The points $u_{i+1/2}^-$ and $u_{i+1/2}^+$ can be computed as:

$$u_{i+1/2}^- = u_i^n + \frac{\Delta z}{2}\left(\frac{\partial f}{\partial z}\right)_i^n \tag{28}$$

$$u_{i+1/2}^{+} = u_{i+1}^{n} - \frac{\Delta z}{2}\left(\frac{\partial f}{\partial z}\right)_{i+1}^{n} \tag{29}$$

where the flux can be evaluated by considering a limiter flux, such as the minmod function [35]:

$$\frac{\partial f}{\partial u} = \text{minmod}\left(\frac{u_{i}^{n} - u_{i+1}^{n}}{\Delta z}, \frac{u_{i-1}^{n} - u_{i}^{n}}{\Delta z}\right) \tag{30}$$

For two inputs, this limiter flux is given by:

$$\text{minmod}(a,b) = \begin{cases} \min\{a,b\} & \text{if } a > 0,\ b > 0 \\ \max\{a,b\} & \text{if } a < 0,\ b < 0 \\ 0 & \text{otherwise} \end{cases} \tag{31}$$

According to Kurganov and Tadmor (2000) [8], the HRCS method offers several advantages over other numerical methods used to solve hyperbolic PDEs: (a) high resolution in discontinuity regions: HRCS is specifically designed to capture discontinuities with high accuracy, avoiding numerical oscillations that are common in traditional discretization methods; (b) simplicity and robustness: by using a central flux approach without the need for complex interpolation or explicit solution reconstruction, HRCS is relatively simple to implement and highly robust; (c) good conservation properties: the method is conservative, meaning that physical quantities such as mass, energy, and momentum are well-preserved throughout the temporal evolution of the solution; (d) broad applicability: HRCS is applicable to a wide range of problems in fluid dynamics, shock waves, and other situations with non-smooth characteristics, such as phase transitions and interfaces.

This strategy has been used to solve problems with different levels of complexity, such as one-dimensional scalar hyperbolic equations, one-dimensional scalar (or systems) hyperbolic conservation laws, one-dimensional convection–diffusion equations, and two-dimensional equations [8]; astrophysical applications considering two-dimensional simulations [36]; one-dimensional and two-dimensional Riemann problems, and the double Mach reflection problem for Euler equations [37].

4. RESULTS AND DISCUSSION

In this section, the numerical methods briefly presented (THINC, WENO and HRCS) are applied. For this purpose, the following points should be highlighted:

- The first case study is purely mathematical and aims to validate each numerical methodology, as well as assess the influence of the number of discretization points and the Courant–Friedrichs–Lewy (CFL) condition [38], defined as:

$$C = \frac{|u|\Delta t}{\Delta z} \tag{32}$$

  where C is the Courant number. Thus, if the constant C, the magnitude of u, and the value of Δz (computed based on the number of discretization points (N) in the spatial direction) are known, the time step size (Δt) can be easily determined. It is important to mention that, for each application, the magnitude of u is computed considering the initial condition.
- To assess the quality of the obtained solution (when the analytical solution is known), the Mean Absolute Error (L_2) is considered:

$$L_2(N) = \left(\frac{1}{N}\sum_{i=1}^{N}\left(U(i) - u(i)\right)^2\right)^{0.5} \tag{33}$$

where $U(i)$ and $u(i)$ represent the analytical and numerical solutions evaluated at the point i, respectively.

- The last two case studies describe classical applications in batch sedimentation, where the function $f(u)$, as well as the initial and boundary conditions, are known.
- All numerical routines were implemented using Scilab® software (version 6.6.1).
- The processing time (PT) is calculated using a Desktop computer with an Intel Core i7-4770 processor and 8GB of memory.

5.1 Burger Equation

First test case considers a classical Burger Equation:

$$\frac{\partial u}{\partial t}+\frac{\partial f(u)}{\partial z}=0,\ 0<z\leq 2\pi,\ 0<t\leq 2 \tag{34}$$

$$f(u)=\frac{1}{2}u^2 \tag{35}$$

$$u(0,z)=0.5+\sin(z) \tag{36}$$

$$u(t,0)=u(t,2\pi)=-0.0435t^3+0.2105t^2-0.4112t+0.4934 \tag{37}$$

As mentioned by Kurganov and Tadmor (2000) [8], this problem presents a shock discontinuity at the critical time t=1. The analytical solution for this problem is given by the evaluation of the following nonlinear equation:

$$u-(0.5+\sin(z-ut))=0 \tag{38}$$

Table 1 shows the L_2 norm at the final time (t=2), and processing time considering the THINC, WENO and HRCS strategies, different number of discretization points and C equal to 0.5.

Table 1: L2 norm for the Burger Equation considering THINC, WENO and HRCS strategies (C=0.5).

		THINC		**WENO**		**HRCS**	
N	Δt	L_2	PT (s)	L_2	PT (s)	L_2	PT (s)
50	4.25×10^{-2}	4.46×10^{-3}	2.18×10^{-2}	1.01×10^{-2}	1.63×10^{-2}	9.95×10^{-3}	1.63×10^{-2}
100	2.10×10^{-2}	2.32×10^{-3}	2.49×10^{-2}	5.19×10^{-3}	1.87×10^{-2}	4.94×10^{-3}	1.87×10^{-2}
200	1.05×10^{-2}	1.67×10^{-3}	2.88×10^{-2}	2.92×10^{-3}	1.95×10^{-2}	2.58×10^{-3}	1.89×10^{-2}
300	6.99×10^{-3}	1.59×10^{-3}	1.49×10^{-1}	2.22×10^{-3}	3.51×10^{-2}	1.87×10^{-3}	1.95×10^{-2}
400	5.24×10^{-3}	1.57×10^{-3}	2.21×10^{-1}	1.91×10^{-3}	5.61×10^{-2}	1.87×10^{-3}	2.26×10^{-2}
500	4.19×10^{-3}	1.37×10^{-3}	2.97×10^{-1}	1.52×10^{-3}	8.97×10^{-2}	5.93×10^{-4}	3.74×10^{-2}
1000	2.09×10^{-3}	3.02×10^{-4}	8.60×10^{-1}	5.39×10^{-4}	3.83×10^{-1}	2.75×10^{-4}	2.06×10^{-1}

In this table it is possible to observe that, for each numerical method, the increase in the number of discretization points (and consequent reduction of the time interval Δt) implies a reduction in the L_2 norm, as expected. On the other hand, there is an increase in the time required for each numerical approach. Regarding each numerical method, it is possible to see that, in terms of the L_2 norm, all results are similar (with alternation between each one). When evaluating the processing time, HRCS presented the best performance.

The influence of the parameter C on obtained results considering N equal to 500 and a final time equal to 2 is presented in Table 2. In this table it is possible to observe that, in terms of L_2 norm, for each numerical approach the results are similar. As observed in the CFL condition (Eq. (32)), the increase of the parameter C implies an increasing of the time interval Δt. Consequently, the processing time also is increased, as expected.

Table 2: L_2 norm for the Burger Equation considering THINC, WENO and HRCS strategies (N=500).

		THINC		WENO		HRCS	
C	Δt	L_2	PT (s)	L_2	PT (s)	L_2	PT (s)
0.5	4.19×10^{-3}	1.37×10^{-3}	2.97×10^{-1}	1.52×10^{-3}	8.97×10^{-2}	5.93×10^{-4}	3.74×10^{-2}
0.6	5.03×10^{-3}	1.40×10^{-3}	2.22×10^{-1}	1.54×10^{-3}	8.75×10^{-2}	5.99×10^{-4}	3.69×10^{-2}
0.7	5.88×10^{-3}	1.42×10^{-3}	2.12×10^{-1}	1.55×10^{-3}	8.67×10^{-2}	6.01×10^{-4}	3.58×10^{-2}
0.8	6.71×10^{-3}	1.43×10^{-3}	2.02×10^{-1}	1.58×10^{-3}	8.55×10^{-2}	6.29×10^{-4}	3.41×10^{-2}
0.9	7.54×10^{-3}	1.48×10^{-3}	1.97×10^{-1}	1.62×10^{-3}	8.34×10^{-2}	6.31×10^{-4}	3.52×10^{-2}

Figure 2 presents the approximate solutions at the post-shock time (t=2) and the 3D profile. In Figures 2a, 2b and 2c, it is possible to observe the quality of the solution obtained by each numerical strategy when compared with the exact solution, i.e., all numerical approaches were able to obtain good estimates when compared with the analytical solution. The 3D profile is shown in Figure 2d, demonstrating the numerical difficulty of this application.

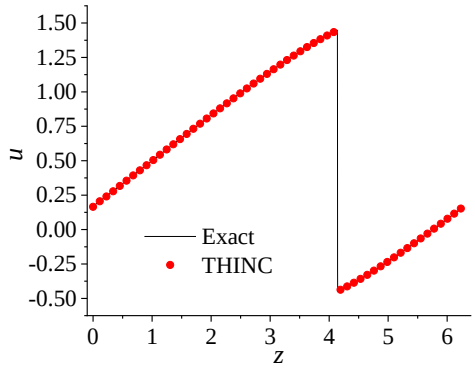

(a) THINC.

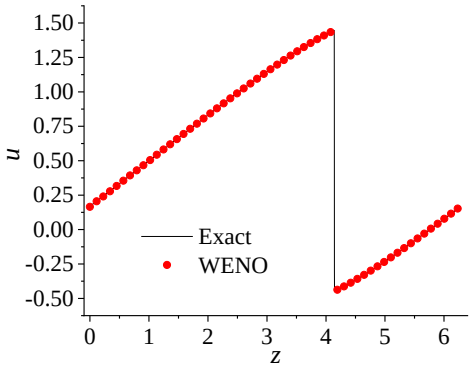

(b) WENO.

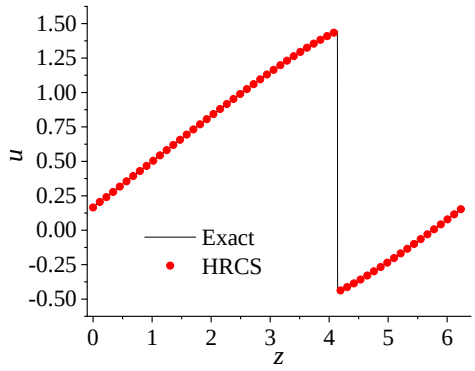

(c) HRCS.

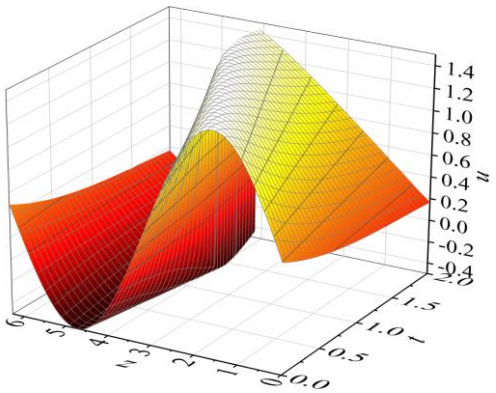

(d) 3D (HCRS strategy).

Figure 2: 2D and 3D profiles considering the THINC, WENO and HRCS strategies (N=500; C=0.5 and t=2).

5.2 Bath Sedimentation (Nocoń, 2010)

The second test case considers a transient one-dimensional modeling of a bath sedimentation process proposed by Nocoń (2010) [39]. In this model, it is assumed that: (i) the velocity of solid particles (v_s) depends only on the local suspended solids concentration; (ii) only the vertical movement of particles is considered; (iii) the horizontal gradients in suspended solids concentration are negligible; and (iv) the movement of solid particles results only from gravitational settling.

For this purpose, the velocity of solids particles is given by Nocón (2010) [39]:

$$v_s(\varepsilon_s) = 4.2\exp(-0.14\varepsilon_s), \text{ [cm/min]} \tag{39}$$

Figure 3 presents the velocity of solid particles and the solids flux density function ($v_s \times \varepsilon_s$) profiles considering Eq. (39) and $0 \leq \varepsilon_s \leq 50$ g/L. These profiles are consistent with expectations, i.e.; initially, the velocity reaches its maximum value, and towards the end of the process (when the concentration reaches its maximum), the velocity becomes zero (since the sediment is compacting at the bottom of the settler, preventing further particle movement). On the other hand, at ε_s equal to 0 and 50 g/L, the solids flux density is approximately zero, as highlighted by Burger et al. (1998) [4].

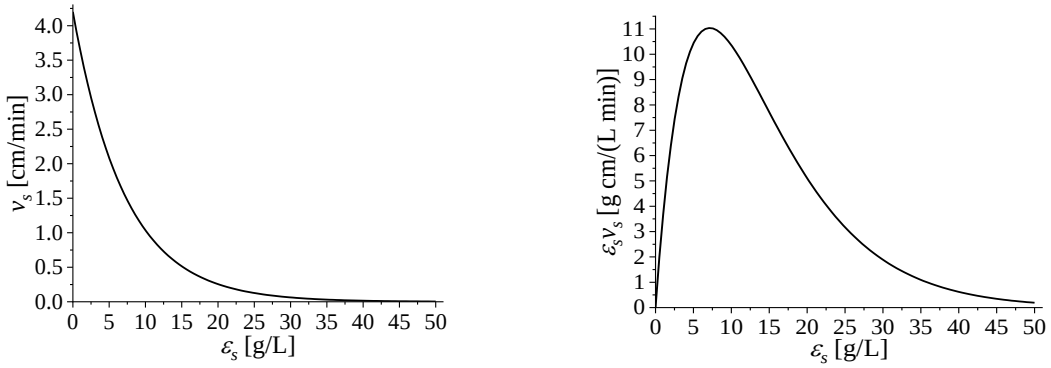

(a) Velocity profile. (b) Solids Flux Density ($v_s \times \varepsilon_s$).

Figure 3: Velocity of solids particles and solids flux density function profiles for the first sedimentation case.

The conservation of mass over the vertical axis (*z*-axis) of the settler and the initial and boundary conditions are given by following partial differential equation:

$$\frac{\partial \varepsilon_s}{\partial t} + \frac{\partial (v_s \varepsilon_s)}{\partial z} = 0, \ 0 < z \leq 80 \text{ cm}, \ 0 < t \leq 30 \text{ min} \tag{40}$$

$$\varepsilon_s(0, z) = \varepsilon_{s0} \text{ g/L} \tag{41}$$

$$\varepsilon_s(t, 0) = \begin{cases} \varepsilon_{s0} \text{ g/L}, & t \leq 0.1 \text{ min} \\ 0 \text{ g/L}, & \text{otherwise} \end{cases} \tag{42}$$

$$\frac{\partial \varepsilon_s(t, 80)}{\partial z} = 0 \tag{43}$$

Equation (41) describes the initial distribution of suspended solids throughout the equipment (this is assumed to be constant and equal to 4 g/L), i.e., the contents of the settler are perfectly mixed at the beginning of the process. The first boundary condition (Eq. (42)) indicates that for *t* less than 0.1, the solids concentration at *z* equal to zero is equal to the initial concentration; otherwise, it is equal to zero. Finally, the second boundary condition (Eq. (43)) states that the solids concentration is maximum when *z* is equal to 80 cm. It is important to note that the condition given by Eq. (42) represents a discontinuity in the solids concentration, complicating the numerical integration of the physical model.

Figure 4 presents the solids concentration profiles at the final time considering the THINC, WENO, and HRCS strategies, different values for the number of discretization points and *C* equal to 0.5. From a physical point of view, the results presented in Figures 4a, 4b and 4c are consistent, i.e.; at time equal to 30 min, the solids concentration throughout most of the settler is zero, reaching its maximum value when *z* is equal to 80 cm (thus satisfying the second boundary condition). This implies that the solid has deposited at the bottom of the settler. For each numerical method, the increase of the number of discretization points implies a change of obtained profiles, demonstrating the effect of this parameter on the solution quality, as expected. Figure 4d presents

a comparison among the profiles obtained for each strategy. Although the profiles observed in this figure are not identical, a concordance between the results obtained by each approach can be observed. This demonstrates that, despite each approach having a different conceptual framework, the results obtained are consistent. Finally, it is important to mention that these results are consistent with those reported by Nocoń (2010) [39], using a numerical strategy based on the discretization of the model with flow control between the layers.

Table 3 presents the processing time for the first sedimentation problem considering all numerical strategies.

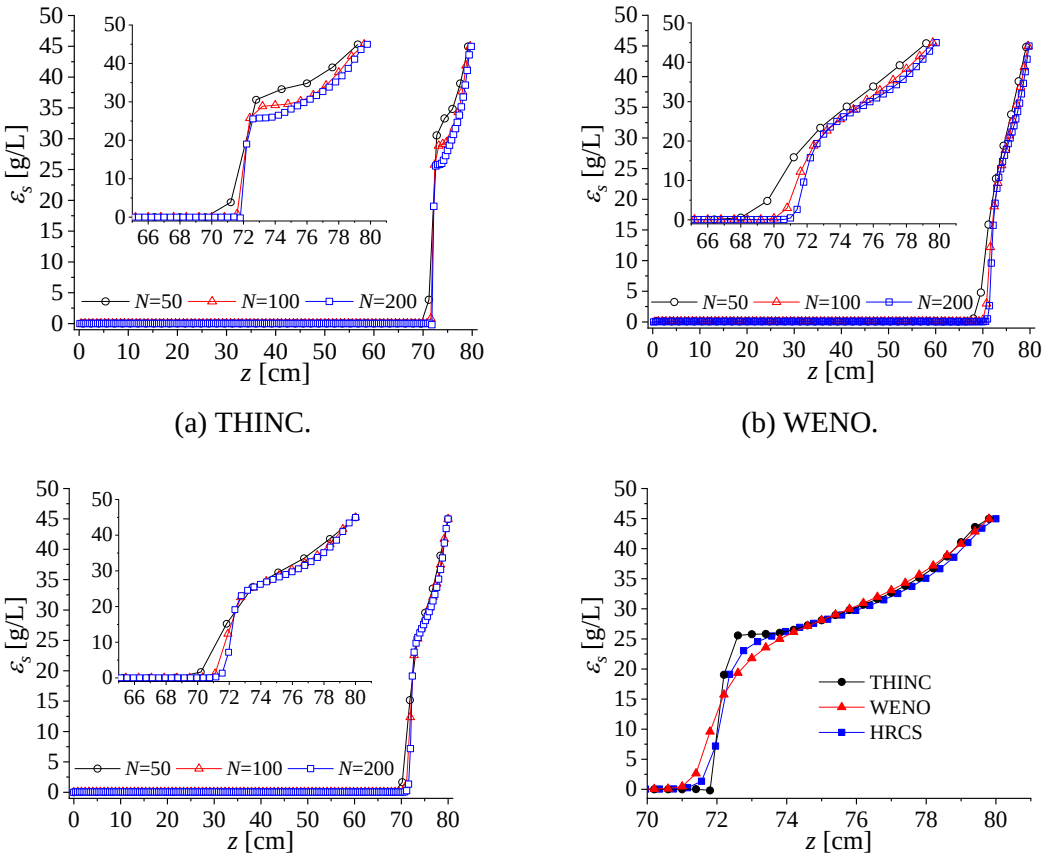

(a) THINC. (b) WENO.

(c) HRCS. (d) THINC, WENO and HCRS (*N*=200).

Figure 4: Solids concentration at final time considering the THINC, WENO and HRCS strategies (C=0.5) for the first sedimentation case.

Table 3: Processing time (s) for the first sedimentation problem considering THINC, WENO and HRCS strategies (C=0.5).

N	Δt	**THINC**	**WENO**	**HRCS**
50	2.55×10^{-3}	1.57	1.69	1.40
100	1.26×10^{-3}	32.43	33.23	30.01
200	6.28×10^{-4}	109.47	105.93	92.33

In this table, an increase in the number of discretization points results in a reduction of the time step (Δt) and an increase in the processing time required to solve the sedimentation problem. Additionally, a significant difference in processing time is observed in each processing time when the value of the parameter *N* is increased. Specifically, compared to THINC, both WENO and HRCS showed a reduction of approximately 3.3% and 15.7%, respectively, when N is equal to 200.

Figure 5 presents the plane and space profiles considering the HRCS strategy for N and C equal to 200 and 0.5, respectively. In Figure 5a, it is possible to observe the evolution of the solids concentration along the settler for different time instances. In this case, as expected, the longer the time, the higher the solids concentration at the bottom of the settler, highlighting the efficiency of this unitary operation. Figure 5b presents the 3D plot of solids concentration as a function of time and length. In this figure, the discontinuity in the profile is evident due to the presence of the three regions: clear (ε_s=0), free settling (ε_s=4 g/L), and compression (4 g/L $\leq \varepsilon_s \leq$ 45 g/L). In the first region, all solid particles have been displaced to the bottom of the settler due to the action of gravity. As a result, the concentration in this region is zero. In the second region, the concentration is equal to initial value (ε_s=4 g/L). Finally, in the third region, there is mass accumulation due to action of gravity. These three regions can also be observed in Figure 5c. The identification of the discontinuity, which is a function of length and time, represents the main numerical challenge in the sedimentation problem. As observed from the results obtained, all the methods considered were able to overcome this difficulty, resulting in physically consistent profiles.

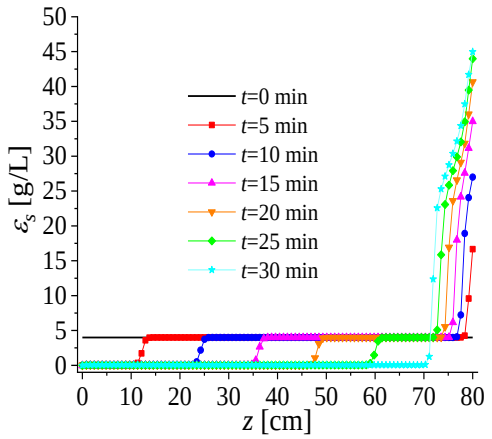

(a) $\varepsilon_s \times z$.

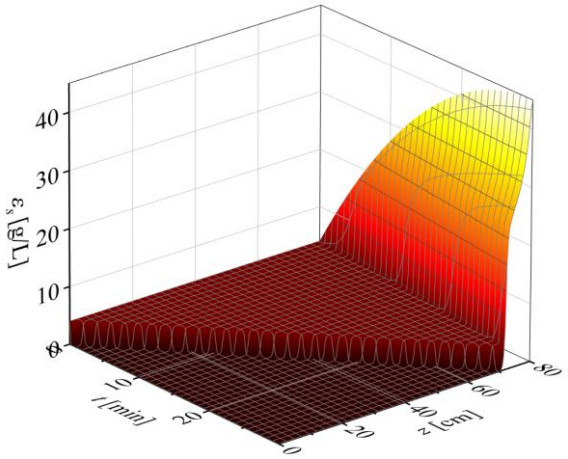

(b) Concentration profile.

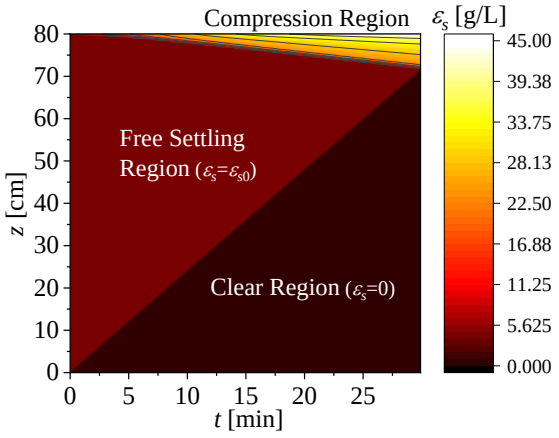

(c) Contour plot.

Figure 5: 2D, 3D, and contour plot profiles considering the HRCS strategy (N=200 and C=0.5). for the first sedimentation case.

5.3 Bath Sedimentation (Diehl, 2015)

The last case considers the bath sedimentation process proposed by Diehl (2015) [20]. The physical modeling is based on the following hypotheses: (i) transient one-dimensional model; (ii) the velocity of solid particles is a function of the local suspended solids concentration; (iii) only the vertical movement of particles is considered; (iv) the horizontal gradients in suspended solids

concentration are negligible; and (v) the movement of solid particles results only from gravitational settling. Mathematically, the model representing this process is given by Diehl (2015) [20]:

$$\frac{\partial \varepsilon_s}{\partial t} + \frac{\partial \left(v_s \varepsilon_s\right)}{\partial z} = 0,\ 0 < z \le 1 \text{ m},\ 0 < t \le 3 \text{ h} \tag{44}$$

$$v_s(\varepsilon_s) = 7.2 \exp\left(-0.5 \varepsilon_s\right),\ [\text{m/h}] \tag{45}$$

$$\varepsilon_s(0, z) = \varepsilon_{s0}\ \text{kg/m}^3 \tag{46}$$

$$\varepsilon_s(t, 0) = \begin{cases} \varepsilon_{s0}\ \text{kg/m}^3, & t \le 0.01 \text{ h} \\ 0\ \text{kg/m}^3, & \text{otherwise} \end{cases} \tag{47}$$

$$\frac{\partial \varepsilon_s(t,1)}{\partial z} = 0 \tag{48}$$

As mentioned in the earlier model, Eq. (46) describes the initial distribution of suspended solids. The first boundary condition (Eq. (47)) indicates that for t less than 0.01, the solids concentration at z equal to zero is equal to the initial concentration (ε_{s0}=4 kg/m^3), otherwise it is equal to zero. The second boundary condition (Eq. (48)), the mass flux is equal to zero.

Figure 6 presents the velocity of solid particles and the solids flux density function ($v_s \times \varepsilon_s$) profiles considering Eq. (45). As highlighted earlier, both the profiles are consistent, i.e., the velocity exhibits a decay behavior with respect to solids concentration, and the solids flux density takes zero values both at ε_s equals to 0 and 20 kg/m^3, respectively [4].

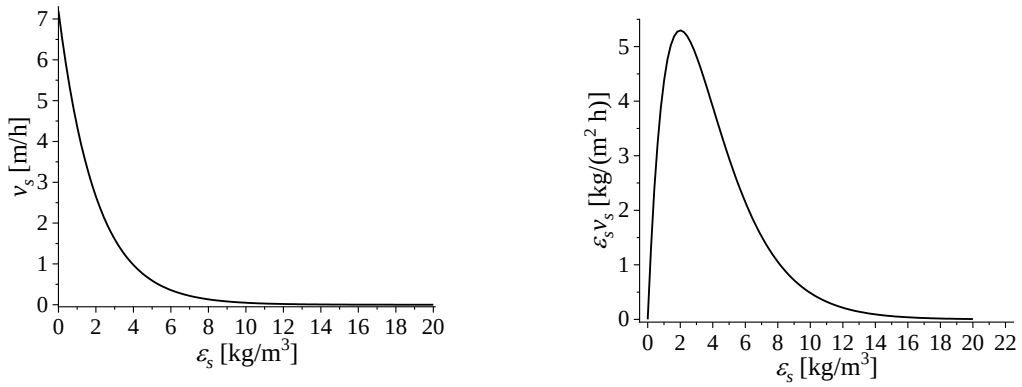

(a) Velocity profile. (b) Solids Flux Density ($v_s \times \varepsilon_s$).

Figure 6: Velocity of solids particles and solids flux density function profiles for the second sedimentation case.

Figure 7a presents the solids concentration profiles at final time considering the THINC, WENO and HRCS strategies and N and C equals to 200 and 0.5, respectively. In this figure, no significant changes are observed among the profiles estimated by each of the approaches considered. Physically, the results are consistent with the expected behavior at the end of the process; i.e., throughout most of the settler, the concentration is zero, while at the bottom, the concentration tends to its maximum value.

Figure 7b presents the temporal evolution of concentration along the settler at different time steps. These profiles demonstrate that the process simulation aligns with the expected physical behavior, as the concentration at the bottom of the settler increases over time, while the concentration at the top decreases proportionally.

Figure 7c presents the 3D plot of solids concentration. In this figure, due to the presence of the three regions: clear (ε_s=0), free settling (ε_s=4 kg/m^3) and compression (4 kg/m^3 $\le \varepsilon_s \le$ ε_{sm}=17 kg/m^3), a discontinuity in the profile can be observed. As mentioned earlier, the first region is characterized by absence of solid particles due to the action of gravity (ε_s=0). In the second

region, the concentration is equal to the initial value (ε_s=4 kg/m^3). In the third region, there is mass accumulation due to action of gravity. These regions can also be observed in Figure 7d. It is important to mention that these results are consistent with those reported by Diehl (2015) [20] using a Godunov's method.

Regarding processing time, when the parameter N is increased (Δt is reduced), the processing time also increases, as shown in Tab. 4. For N equal to 200, a reduction of approximately 17.5% and 26.3% for both WENO and HRCS compared to THINC is observed.

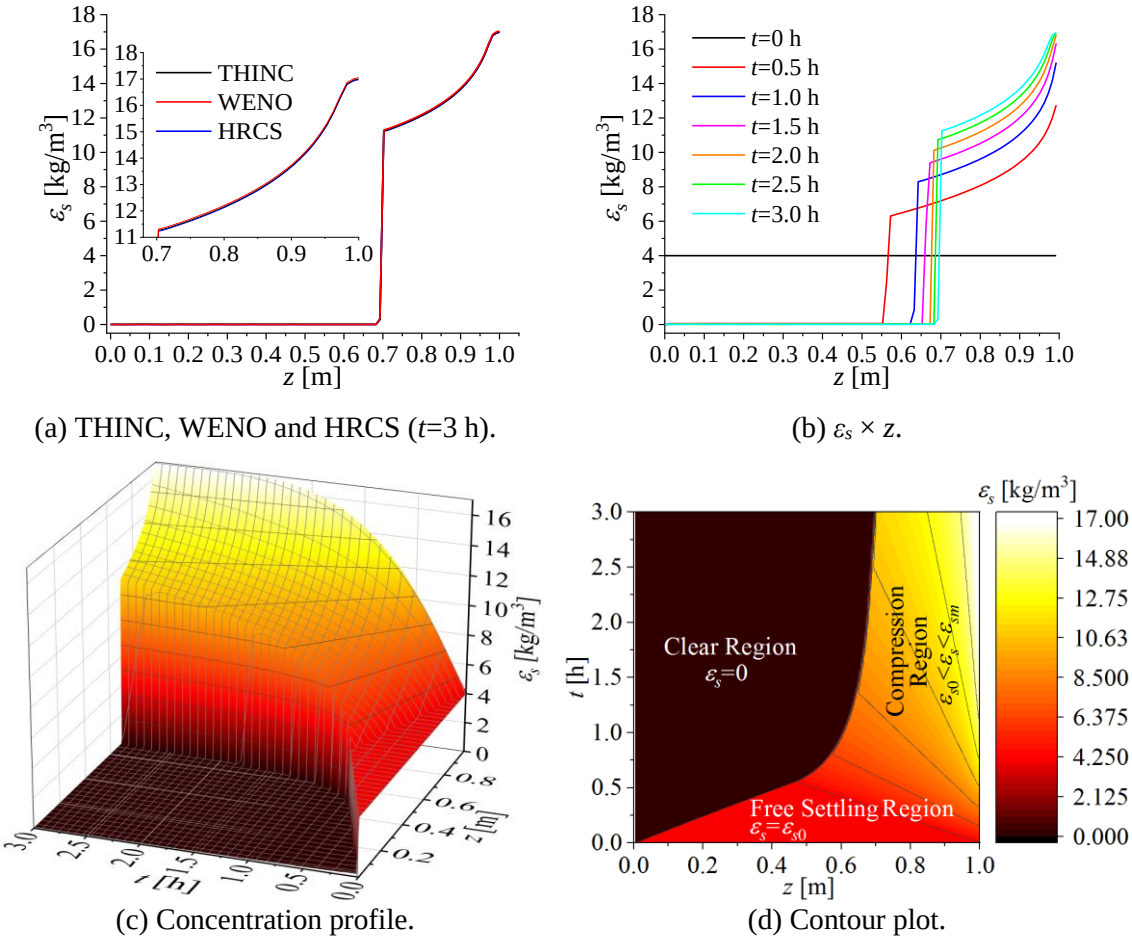

(a) THINC, WENO and HRCS (t=3 h).

(b) $\varepsilon_s \times z$.

(c) Concentration profile.

(d) Contour plot.

Figure 7: 2D, 3D and contour plot considering the HRCS strategy (N=200 and C=0.5) for the second sedimentation case.

Table 4: Processing time (s) for the second sedimentation problem considering THINC, WENO and HRCS strategies (C=0.5).

N	Δt	THINC	WENO	HRCS
50	2.55×10^{-3}	0.53	0.68	0.44
100	1.26×10^{-3}	2.07	2.73	1.89
200	6.28×10^{-4}	8.89	7.33	6.56

5. CONCLUSIONS

In this work, three numerical approaches—Tangent of Hyperbola Interface Capturing (THINC), Weighted Essentially Non-Oscillatory (WENO), and High-Resolution Central Scheme (HRCS)—were employed to solve a classical chemical engineering problem exhibiting discontinuities: the simulation of the particle sedimentation process. The results demonstrated that all three numerical strategies were capable of providing accurate estimates of the solid

concentration profiles. Moreover, the results were physically consistent with those reported in the literature. As expected, increasing the number of discretization points led to a higher processing time required to solve the problem. The parameter C required by the Courant–Friedrichs–Lewy condition should be chosen by the user. However, it can be easily defined based on preliminary simulations. Finally, in terms of computational efficiency, the best results were obtained using the HRCS approach. Processing time evaluation is crucial for parameter estimation and engineering system design.

It is important to emphasize that the velocity functions considered in engineering applications were proposed in the literature to characterize a specific type of sedimentation. In this context, for the analysis of a new case study, it is necessary to know the velocity function or solve the model described by the momentum balance.

Future work suggestions include: (i) solving the sedimentation problem by considering the momentum equation; (ii) extending each numerical approach to solve multidimensional problems; (iii) estimating solid flow densities using real experimental data; (iv) investigating the Boycott phenomenon in inclined settlers; (v) evaluating the effect of temperature on particle sedimentation; and (vi) exploring the type of batch test (Kynch or Diehl).

6. ACKNOWLEDGMENTS

Dr. Lobato acknowledges the Brazilian agency CNPq for the financial support to his research through the award of a research scholarship (grant number 309178/2023-1).

7. REFERENCES

1. Agarwal A, Liu Y. Remediation technologies for oil-contaminated sediments. Mar Pollut Bull. 2015 Dec;101(2):483-90. doi: 10.1016/j.marpolbul.2015.09.010
2. Sun L, Fang C, Li F, Zhu R, Zhang Y, Yuan X, et al. Innovations and challenges of sedimentology in oil and gas exploration and development. Pet Explor Dev. 2015 Apr;42(2):143-51. doi: 10.1016/S1876-3804(15)30001-X
3. Hilgert S, Sotiri k, Fuchs S. Review of methods of sediment detection in reservoirs. Int J Sediment Res. 2024 Feb;39(1):28-43. doi: 10.1016/j.ijsrc.2023.12.004
4. Bürger R, Concha F. Mathematical model and numerical simulation of the settling of flocculated suspensions. Int J Multiphase Flow. 1998 Sep;24:1005-23. doi: 10.1016/S0301-9322(98)00026-3
5. Bürger R, Concha F, Tiller FM. Applications of the phenomenological theory to several published experimental cases of sedimentation processes. Chem Eng J. 2000 Dec;80:105-17. doi: 10.1016/S1383-5866(00)00090-3
6. Bürger R, Damasceno JJR, Karlsen KH. A mathematical model for batch and continuous thickening of flocculated suspensions in vessels with varying crosssection. Int J Miner Process. 2004 Feb;73:183-208. doi: 10.1016/S0301-7516(03)00073-5
7. Tao W, Wu J, Wang Q. Mathematical model of sediment and solute transport along slope land in different rainfall pattern conditions. Sci Rep. 2017 Mar;7:44082. doi: 10.1038/srep44082
8. Kurganov A, Tadmor E. New high-resolution central schemes for nonlinear conservation laws and Hamilton-Jacobi equations. J Comput Phys. 2000;160(2):241-82. doi: 10.1006/jcph.2000.6459
9. Friedrichs KO. Symmetric hyperbolic linear differential equations. Commun Pure Appl Math. 1954 May;7:345. doi: 10.1002/cpa.3160070206
10. Van Leer B. Towards the ultimate conservative difference scheme. A second-order sequel to Godunov's method. J Comput Phys. 1979 Jul;32:101-36. doi: 10.1016/0021-9991(79)90145-1
11. Nessyahu H, Tadmor E. Non-oscillatory central differencing for hyperbolic conservation laws. J Comput Phys. 1990 Apr;87:408. doi: 10.1016/0021-9991(90)90260-8
12. Liu X-D, Osher S, Chan T. Weighted essentially non-oscillatory schemes. J Comput Phys. 1994 Nov;115(1):200-12. doi: 10.1006/jcph.1994.1187
13. Xiao F, Honma Y, Kono Y. A simple algebraic interface capturing scheme using hyperbolic tangent function. Int J Numer Methods Fluids. 2005 Apr;48:1023-40. doi: 10.1002/fld.975
14. Bürger R, García A, Karlsen KH, Towers JD. A family of numerical schemes for kinematic flows with discontinuous flux. J Eng Math. 2008 Sep;60:387-425. doi: 10.1007/s10665-007-9148-4
15. Bürger R, Karlsen KH, Towers, JD. An Engquist–Osher-type scheme for conservation laws with discontinuous flux adapted to flux connections. SIAM J. Numer Anal. 2009 Apr;47(3):1684-712. doi: 10.1137/07069314X

16. Wang S, Guo Y, Hu Y. Mathematics model of sedimentation and application in industrial sedimentation. IEEE. 2010 Nov;1-5. doi: 10.1109/iceee.2010.5660549
17. Bürger R, Careaga J, Diehl S. A review of flux identification methods for models of sedimentation. Water Sci Technol. 2020 Apr;81(8):1715-22. doi: 10.2166/wst.2020.113
18. Diehl S. Estimation of the batch-settling flux function for an ideal suspension from only two experiments. Chem Eng Sci. 2007 Sep;17:4589-601. doi: 10.1016/j.ces.2007.05.025
19. Bürger R, Diehl S, Farås S, Nopens I, Torfs E. A consistent modelling methodology for secondary settling tanks: a reliable numerical method. Water Sci Technol. 2013 Jul;68(1):192-208. doi: 10.2166/wst.2013.239
20. Diehl S. Numerical identification of constitutive functions in scalar nonlinear convection–diffusion equations with application to batch sedimentation. Appl Numer Math. 2015 Sep;95:154-72. doi: 10.1016/j.apnum.2014.04.002
21. Rocha RR, Oechsler BF, Meleiro LAC, Fagundes FM, Arouca FO, Damasceno JJR, et al. Settling of weighting agents in non-Newtonian fluids to off-shore drilling wells: Modeling, parameter estimation and analysis of constitutive equations. J Pet Sci Eng. 2020 Jan;184:106535. doi: 10.1016/j.petrol.2019.106535
22. Peçanha, R. Sistemas particulados: operações unitárias envolvendo partículas e fluidos. 1 ed. Rio de Janeiro (RJ): Elsevier; 2014.
23. Fagundes FM, Oliveira GG, Santos NBC, Damasceno JJR, Arouca FO. Gravitational settling of calcium carbonate in different non-Newtonian carboxymethyl cellulose concentrations using the gamma-ray attenuation technique. Chem. Eng. Sci. 2021 Mar:232:116367. doi: 10.1016/j.ces.2020.116367.
24. Bürger R, Wendland WL. entropy boundary and jump conditions in the theory of sedimentation with compression. Math Methods Appl. Sci. 1998 Dec;21:865-82. doi: 10.1002/(SICI)1099-1476(199806)21:9<865::AID-MMA983>3.0.CO;2-9
25. Xiao F, Ii S, Chen C. Revisit to the THINC scheme: A simple algebraic VOF algorithm. J Comput Phys. 2011 Aug;230(19):7086-92. doi: 10.1016/j.jcp.2011.06.012
26. Ii S, Xie B, Xiao F. An interface capturing method with a continuous function: The THINC method on unstructured triangular and tetrahedral meshes. J Comput Phys. 2014 Feb;259:260-9. doi: 10.1016/j.jcp.2013.11.034
27. Xie B, Ii S, Xiao F. An efficient and accurate algebraic interface capturing method for unstructured grids in 2 and 3 dimensions: The THINC method with quadratic surface representation. Int J Numer Methods Fluids. 2014 Oct;76(12):1025-42. doi: 10.1002/fld.3968
28. Deng X, Xie B, Loubère R, Shimizu Y, Xiao F. Limiter-free discontinuity-capturing scheme for compressible gas dynamics with reactive fronts. Comput Fluids, 2018 Jul;171:1-14. doi: 10.1016/j.compfluid.2018.05.015
29. Jiang S, Shu C-W. Efficient implementation of weighted ENO schemes. J Comput Phys. 1996 Jun;126(1):202-28. doi: 10.1006/jcph.1996.0130
30. Shu CW. Advanced numerical approximation of nonlinear hyperbolic equations. Lecture notes in mathematics. In: Quarteroni A, editor. Essentially non-oscillatory and weighted essentially non-oscillatory schemes for hyperbolic conservation laws. Heidelberg (Germany): Springer Berlin; 1998. p. 325-432.
31. Shu C-W. Essentially non-oscillatory and weighted essentially non-oscillatory schemes. Acta Numer. 2020 Nov;29:701-62. doi: 10.1017/S0962492920000057
32. Shu C-W. High order weighted essentially nonoscillatory schemes for convection dominated problems. SIAM Rev. 2009 Feb;51(1):82-126. doi: 10.1137/070679065
33. Frenzel D, Lang J. A third-order weighted essentially non-oscillatory scheme in optimal control problems governed by nonlinear hyperbolic conservation laws. Comput Optim Appl. 2021 Jul;80:301-20. doi: 10.1007/s10589-021-00295-2
34. Adebayo EM, Tsoutsanis P, Jenkins KW. Application of central-weighted essentially non-oscillatory finite-volume interface-capturing schemes for modeling cavitation induced by an underwater explosion. Fluids, 2024 Jan;9(2):33. doi: 10.3390/fluids9020033
35. Roe P. Characteristic-based schemes for the Euler equations. Ann Rev Fluid Mech. 1986 Jan;18:337-65. doi: 10.1146/annurev.fl.18.010186.002005
36. Lucas-Serrano A, Font JA, Ibáñez JM, Martí JM. Assessment of a high-resolution central scheme for the solution of the relativistic hydrodynamics equations. Astron Astrophys. 2004 Nov;428(2):703-15. doi: 10.1051/0004-6361:20035731
37. Cai Z, Li D, Hu Y, Li M, Meng X. High resolution central scheme using a new upwind slope limiter for hyperbolic conservation laws. Comput Fluids. 2021 Dec;231:105164. doi: 10.1016/j.compfluid.2021.105164
38. Courant R, Friedrichs K, Lewy H. On the partial difference equations of mathematical physics. Math. Ann.1928 Sep;100:32-74.

39. Nocoń W. Practical aspects of batch sedimentation control based on fractional density changes. Powder Technol. 2010 Feb;198(1):167-74. doi: 10.1016/j.powtec.2009.11.007